AGU PUBLICATIONS

Geophysical Research Letters

RESEARCH LETTER

10.1002/2016GL069878

Key Points:
- Two distinct chromophores have been detected in the dark global ocean
- A chromophore centered at 302 nm is due to the secondary absorption peak of nitrate
- A chromophore centered at 415 nm is presumably due to cytochrome c and can be a used as proxy for cumulative respiration

Supporting Information:
- Figure S1
- Table S1
- Supporting Information S1

Correspondence to:
T. S. Catalá,
teresascatala@gmail.com;
teresc@ugr.es

Citation:
Catalá, T. S., I. Reche, C. L. Ramón, À. López-Sanz, M. Álvarez, E. Calvo, and X. A. Álvarez-Salgado (2016), Chromophoric signatures of microbial by-products in the dark ocean, *Geophys. Res. Lett.*, *43*, 7639–7648, doi:10.1002/2016GL069878.

Received 3 JUN 2016
Accepted 11 JUL 2016
Accepted article online 14 JUL 2016
Published online 30 JUL 2016

Chromophoric signatures of microbial by-products in the dark ocean

Teresa S. Catalá[1,2], Isabel Reche[1], Cintia L. Ramón[1], Àngel López-Sanz[3], Marta Álvarez[4], Eva Calvo[3], and Xosé A. Álvarez-Salgado[2]

[1]Departamento de Ecología and Instituto del Agua, Universidad de Granada, Granada, Spain, [2]CSIC Instituto de Investigacións Mariñas, Vigo, Spain, [3]CSIC Institut de Ciencies del Mar, Barcelona, Spain, [4]IEO Centro Oceanográfico de A Coruña, Coruña, Spain

Abstract Detailed examination of the absorption spectra from dark ocean samples allowed us to identify and deconvolve two distinct chromophores centered at 302 nm (UV) and 415 nm (visible) from the exponential decay curve characteristic of humic substances. The UV chromophore was ubiquitous in intermediate and deep waters, and it has been proposed as the secondary absorption peak of nitrate. The visible chromophore was prominent at the central and intermediate water masses of the North Pacific, and it has been proposed as cytochrome c. Subtraction of the modeled absorption spectra of the two chromophores from the measured absorption spectrum of the samples leads to a spectral slope overestimation by 13.3 ± 6.0% for $S_{275-295}$ and 14.8 ± 10.6% for $S_{350-400}$. To only consider the chromophoric fraction of DOM, the absorption spectra of nitrate should be subtracted in samples with a $[NO_{3-}]$:a_{302} ratio > 70 μM m.

1. Introduction

Oceanic dissolved organic matter (DOM) represents one of Earth's largest reservoirs of reduced carbon, and most of it (>95%) is in the form of recalcitrant DOM (RDOM), being resistant to microbial degradation [*Hansell and Carlson*, 2013]. Although the labile organic matter from photosynthesis is preferentially respired back to CO_2 in the surface ocean, a minor fraction of it is transformed into RDOM as a by-product of the microbial metabolism thereby preserving fixed carbon in the ocean [*Ogawa et al*., 2001; *Benner and Herndl*, 2011; *Lechtenfeld et al*., 2015]. This process has been recently termed microbial carbon pump [*Jiao et al*., 2010], having implications for climate as it could contribute to the sequestration of atmospheric CO_2 at centennial to millennial time scales.

A portion of the DOM pool absorbs UV and visible light and has been known as chromophoric DOM (CDOM). It has been widely used as an "optical marker" in ocean hydrography and biogeochemistry studies [*Stedmon and Nelson*, 2015]. Light absorption by any organic functional group capable of absorbing light (chromophore) is characterized by its intensity and shape. While the intensity results from the molar absorption and concentration of the chromophore, the shape of light absorption (wavelength maxima and band width) depends on the electronic transitions involved [*Stedmon and Nelson*, 2015].

Absorption spectra of natural waters provide both quantitative and qualitative information on CDOM in aquatic environments. Absorption coefficients at specific wavelengths, a_λ, are used as proxies of the concentration of CDOM, and a wide variety of spectral indices and slopes have provided key information on the origin and molecular structure of CDOM [*Twardowski et al*., 2004; *Helms et al*., 2008]. Most of the research efforts have focused on the characterization of the exponential decay of a_λ with increasing wavelength, traditionally associated with dissolved humic substances [*Bricaud et al*., 1981]. In fact, recent studies by *Nelson et al*. [2010] and lately by *Catalá et al*. [2015] presented conventional absorption coefficients and spectral slopes for global ocean CDOM to make them comparable with previous works. However, detailed inspection of CDOM spectra from open ocean waters have been scarcely performed, resulting in the identification of a specific chromophore at 415 nm [*Röttgers and Koch*, 2012] and the recent development of a method, based on a Gaussian decomposition of the absorption spectra, that distinguishes specific chromophores [*Massicotte and Markager*, 2016]. Here we thoroughly explore a collection of 740 CDOM spectra from the dark global ocean (water depths > 200 m) and identified two distinct chromophores, centered at 302 nm and 415 nm, by statistically isolating the absorption coefficient signal attributable to these chromophores from the standard decreasing exponential curve due to the pool of humic substances. Second, we assessed the impact of these

chromophores on the traditional description of CDOM spectra based on absorption coefficients at specific wavelengths and spectral slopes over defined ranges. And third, we applied a water mass analysis that allowed us to quantify and explain the prevalence of both chromophores in the most abundant water masses of the dark global ocean.

2. Materials and Methods

The Malaspina 2010 circumnavigation was conducted from December 2010 to July 2011 on board R/V *Hespérides* along the Atlantic, Indian, and Pacific Oceans, spanning latitudes from 34°N to 40°S. During the cruise, 147 hydrographic stations were occupied (Figure 1a). The water column was sampled from the surface to 4000 m depth with a 24–10 L Niskin bottles rosette sampler. Continuous conductivity-temperature-depth and dissolved oxygen profiles were recorded with a Seabird 911+ conductivity-temperature-depth (CTD) probe equipped with a redundant temperature and salinity sensor for intercomparison and a polarographic membrane oxygen sensor Seabird SBE-43. Temperature and pressure sensors were calibrated at the SeaBird laboratory before the circumnavigation. Onboard salinity calibration was carried out with a Guildline AUTOSAL model 8410 A salinometer with a precision better than 0.002 for single samples and the potentiometric end point Winkler method for the calibration of the oxygen sensor. Oxygen saturation was calculated from practical salinity and potential temperature with the equation of *Benson and Krauss* [1984]. Apparent oxygen utilization (AOU) was calculated as the difference between the saturation and measured dissolved oxygen concentrations. Nitrate was measured on board by segmented flow analysis with colorimetric detection [*Grasshoff et al*., 1999].

2.1. CDOM Absorption Coefficient Spectra

At each station, samples for the determination of the absorption spectra of CDOM were taken from eight discrete depths between 200 and 4000 m depth, poured directly from the Niskin bottle into acid cleaned 250 mL glass flasks and immediately stored in the dark until analysis on board within a few hours after collection. Samples were not filtered because light absorption due to pigments and detrital particles contribute only to a minor fraction of the open ocean CDOM absorption at depth [*Nelson et al*., 1998, 2007], and they are hardly detectable even with the highly sensitive point-source integrating cavity absorption meter [*Röttgers and Koch*, 2012].

The UV-visible absorbance of CDOM was determined from 250 to 750 nm at 1 nm intervals in 10 cm path length quartz cuvettes in a double beam Perkin Elmer lambda 850 spectrophotometer, and a blank was measured every five samples to detect and correct (linearly) any instrument drift. The estimated detection limit of this spectrophotometer for quantifying CDOM absorption is 0.001 absorbance units or 0.02 m^{-1}. The absorbance was converted into Naperian absorption coefficient (m^{-1}) using the equation

$$a_\lambda = 2.303 \frac{\left[\mathrm{Abs}_{(\lambda)} - \mathrm{Abs}_{(600-750)}\right]}{l} \quad (1)$$

where $\mathrm{Abs}_{(\lambda)}$ is the absorbance at a given wavelength (nm), $\mathrm{Abs}_{(600-750)}$ is the average absorbance between 600 and 750 nm, l is the path length of the cuvette (0.1 m), and 2.303 is the factor that converts from decadic to natural logarithms. During the measurements, we first checked that the differences between sample and baseline absorbance at long wavelengths (>600 nm) was < 0.0005 absorbance units. In the case that difference was > 0.0005 absorbance units, we renewed the water in the sample cuvette and repeated the measurement. In most cases, we achieved a final difference < 0.0005 absorbance units. To correct this generally minor effect of light scattering by particles and microbubbles, we applied a wavelength-independent correction [*Green and Blough*, 1994] by subtracting the mean absorbance from 600 to 750 nm from all spectral absorbance values (equation (1)).

2.2. Chromophore Identification Analysis

To locate and quantify the chromophores centered at 302 nm (UV chromophore) and 415 nm (visible light spectrometer (VIS) chromophore) (Figure S1 in the supporting information), we developed a MATLAB toolbox (http://ecologia.ugr.es/pages/herramientas/toolbox-matlab?lang=en) to obtain the parameters that best fit (least squares sense) the following equation [*Röttgers and Koch*, 2012; *Breves et al*., 2003]:

$$a_\lambda = b_1 \mathrm{e}^{-b_2(\lambda-\lambda_0)} + b_3 \frac{1}{\sigma\sqrt{2\pi}} e^{\frac{-(\lambda-\lambda_0)^2}{2\sigma^2}} + b_4 \quad (2)$$

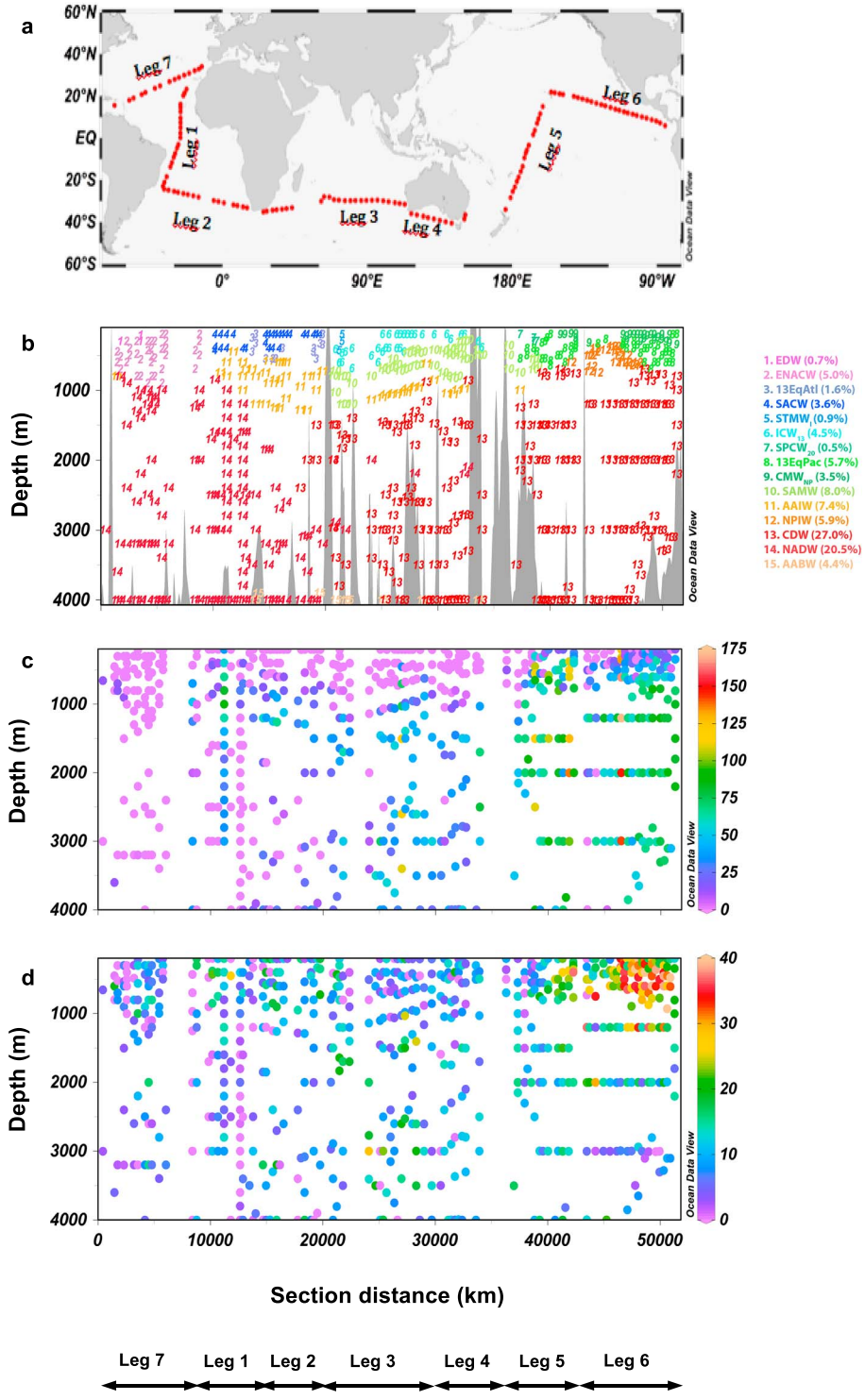

Figure 1. Cruise track of the Malaspina 2010 circumnavigation and global distribution of the water types (WT) and the absorption coefficient of the chromophores. (a) Cruise track of the Malaspina 2010 circumnavigation on board the Spanish R/V *Hespérides*; Distribution of (b) the most abundant fifteen WT domains sampled during the Malaspina 2010 circumnavigation; (c) absorption coefficients of the UV chromophore ($a_{\text{Ch-UV}}$, $\times 10^{-3}$ m^{-1}), $N = 740$; and (d) absorption coefficients of the Visible chromophore ($a_{\text{Ch-VIS}}$, $\times 10^{-3}$ m^{-1}), $N = 713$. Note that the depth scale starts at 200 m. Produced with Ocean Data View [*Schlitzer*, 2016].

The equation was fitted within different wavelength ranges for each chromophore. The first and third terms of the equation models the exponential decay with increasing wavelength characteristic of the signature of humic substances in the CDOM spectrum of any natural sample. It consists of a preexponential term (b_1), an exponential slope (b_2), and an absorption parameter to correct for offsets in the absorption at longer wavelength (b_4). The second term is a Gaussian function to model the absorption spectra of the UV or VIS chromophore, with b_3 being the height at the reference wavelength λ_o of the chromophore. λ_o is the maximum wavelength of the UV or VIS chromophores and σ the width of the Gaussian function. The absorption coefficient of the UV or VIS chromophores at their respective λ_o ($a_{Ch\text{-}UV}$ or $a_{Ch\text{-}VIS}$) is calculated as $b_3 \frac{1}{\sigma\sqrt{2\pi}}$. b_1, b_2, b_3, b_4, λ_0, and σ are optimized with the MATLAB toolbox. To optimize the λ_o and σ of the UV chromophore, values from 280 nm to 320 nm at 5 nm intervals were tested for λ_o and from 15 nm to 30 nm at 5 nm intervals for σ. For the case of the VIS chromophore, the ranges were from 390 nm to 440 nm at 5 nm intervals for λ_o and again from 15 to 30 nm at 5 nm intervals for σ. Equation (2) was applied to the wavelength range from 250 to 400 nm to obtain the parameters of the UV chromophore and from 350 to 600 nm to obtain the parameters of the VIS chromophore.

2.3. Ideal Water Ages

The ideal water ages were estimated by interpolating the gridded mean ages obtained by *Khatiwala et al*. [2009, 2012] to our sample time, locations, and depths. These ages represent the time elapsed from the instant that each water samples was last in contact with the atmosphere. For more details see *Catalá et al*. [2015].

2.4. Water Mass Analysis

The sampling strategy of selecting depths according to extreme values of salinity, potential temperature, and dissolved oxygen allowed us to secure a collection of the most representative water masses of the world ocean. A classical triangular mixing analysis involving salinity, potential temperature, and volume conservation equations was applied by *Catalá et al*. [2015] to obtain the water mass composition of every sample collected during the circumnavigation. A total of 22 water types (Table 1) were identified and their respective proportions on each sample were calculated. The proportion of the total volume of water sampled that corresponds to water type i (%VOL$_i$) was calculated as % VOL$_i = \sum_j x_{ij}/n$, where x_{ij} is the percentage of water type i in sample j and n the number of samples. Next, we obtained the archetypal value of variable N (N_i)—defined as the water mass proportion weighted average value of N in water type i and calculated as $\sum_j (x_{ij} \cdot N_j)/\sum_j x_{ij}$, where N_j is the value of N in sample j [*Catalá et al*., 2015]—and its corresponding standard deviation (SDN$_i$)—calculated as $\sqrt{\sum_j x_{ij} \cdot (N_j - N_i)^2 / \sum_j x_{ij}}$—for each one of the 22 water types. Archetype values retain information about the variability of N that can be attributed to mixing of water types and basin-scale mineralization processes from the site where the water types were defined to their respective centers of mass along the circumnavigation [*Álvarez-Salgado et al*., 2013]. Here we obtained archetype values (N_i) for the water depth (z_i), ideal age (τ_i), apparent oxygen utilization (AOU$_i$), nitrate (NO$_{3i}$), absorption coefficients of the UV ($a_{Ch\text{-}UVi}$), and VIS ($a_{Ch\text{-}VISi}$) chromophores, and spectral slopes of the measured ($S_{275–295i}$, $S_{350–400i}$, and $S_{250–500i}$), and chromophore-subtracted (Sc$_{275–295i}$, Sc$_{350–400i}$, and Sc$_{250–500i}$) absorption spectra (Table 1).

The division of the archetypal AOU (in μmol kg^{-1}) by the archetypal τ (in years) provides a measure of the archetypal oxygen utilization rate (OUR$_i$) of each water mass (Table 1), an indicator of the rate at which the metabolism of organic matter occurs in oxygenic environments [*Jenkins*, 1982].

3. Results and Discussion

3.1. Water Masses Distribution

The water types (WT) sampled during the circumnavigation were classified into central (200–500 m), intermediate (500–1500 m), and abyssal (>1500 m) according to their depth range, representing 26%, 22%, and 52% of the total sampled volume, respectively (Table 1 and Figure 1b). Central waters originate at temperate latitudes and are restricted to the oceanic area where they are formed. The most abundant central WT during the Malaspina circumnavigation was the 13°C water of the Equatorial Pacific (13EqPac) with around 6% of the total sampled volume. Regarding intermediate waters, their sources are at subpolar latitudes, except for the case of the Mediterranean Water (MW), which spills out from the Strait of Gibraltar with elevated salinity and

Geophysical Research Letters

10.1002/2016GL069878

Table 1. Archetypal Values of Hydrographical and Biogeochemical Parameters, Distinct Chromophore Absorptions, and Spectral Slopes Corresponding to the Different Water Types (WT) Intercepted During the Circumnavigation[a]

Domain	Acronym	VOL_i (%)	Z_i (m)	AOU_i ($\mu mol\ kg^{-1}$)	τ_i (years)	OUR_i ($\mu mol\ kg^{-1}\ yr^{-1}$)	NO_{3i} (μM)	$a_{Ch\text{-}UVi}$ ($10^{-3}\ m^{-1}$)	$a_{Ch\text{-}VISi}$ ($10^{-3}\ m^{-1}$)	NO_{3i}/a_{302i} ($\mu M/m^{-1}$)	$a_{Ch\text{-}UVi}/a_{302i}$ (%)	$a_{Ch\text{-}VISi}/a_{415i}$ (%)	$Sc_{275-295i}$ (μm^{-1})	$Sc_{350-400}$ (μm^{-1})	% Increment $S_{275-295i}$	% Increment $S_{350-400i}$
Central	EDW	0.7%	264 ± 20	46 ± 8	11 ± 4	4.0 ± 2.0	7.9 ± 1.5	0 ± 0	6 ± 2	19.0 ± 3.7	0 ± 0	5 ± 4	28 ± 2	10 ± 1	0 ± 15	13 ± 22
(200–500 m)	$ENACW_{12}$	3.2%	641 ± 40	114 ± 7	103 ± 9	1.1 ± 0.2	22.6 ± 1.6	3 ± 2	5 ± 1	59.4 ± 5.0	1 ± 1	5 ± 2	25 ± 1	13 ± 1	3 ± 10	24 ± 13
	$ENACW_{15}$	1.8%	327 ± 25	63 ± 8	28 ± 7	2.3 ± 0.9	11.9 ± 1.6	0 ± 0	7 ± 1	32.0 ± 5.0	0 ± 0	6 ± 3	28 ± 1	10 ± 1	0 ± 10	1 ± 20
	13EqAtl	1.6%	427 ± 37	61 ± 7	134 ± 18	0.5 ± 0.1	16.7 ± 1.9	2 ± 2	9 ± 1	66.9 ± 9.6	1 ± 1	17 ± 7	30 ± 2	14 ± 2	1 ± 12	9 ± 33
	$SACW_{12}$	2.2%	303 ± 26	110 ± 16	104 ± 16	1.1 ± 0.3	19.3 ± 2.8	7 ± 4	10 ± 1	55.5 ± 8.8	2 ± 1	14 ± 5	27 ± 1	10 ± 1	1 ± 9	6 ± 14
	$SACW_{18}$	1.4%	211 ± 11	38 ± 12	21 ± 9	1.8 ± 1.3	6.9 ± 2.2	1 ± 2	9 ± 2	17.4 ± 4.0	0 ± 1	12 ± 5	32 ± 2	12 ± 1	3 ± 11	26 ± 19
	$STMW_I$	0.9%	259 ± 35	26 ± 3	14 ± 17	1.9 ± 2.4	17.6 ± 1.1	0 ± 0	9 ± 2	28.0 ± 4.8	0 ± 0	18 ± 8	36 ± 2	15 ± 1	1 ± 10	29 ± 20
	ICW_{13}	4.5%	395 ± 28	32 ± 2	51 ± 12	0.6 ± 0.2	6.1 ± 1.4	1 ± 1	8 ± 1	48.0 ± 4.5	0 ± 0	14 ± 4	34 ± 1	14 ± 1	1 ± 5	21 ± 15
	$STMW_{SP}$	0.2%	269 ± 26	49 ± 11	58 ± 54	0.9 ± 1.0	1.3 ± 0.8	1 ± 3	6 ± 3	68.2 ± 3.2	1 ± 2	21 ± 27	40 ± 7	10 ± 1	0 ± 34	22 ± 15
	$SPCW_{20}$	0.5%	277 ± 84	70 ± 15	44 ± 21	1.6 ± 1.1	10.5 ± 0.8	12 ± 12	4 ± 2	35.4 ± 6.4	5 ± 6	7 ± 9	34 ± 4	12 ± 2	3 ± 25	11 ± 33
	13EqPac	5.7%	483 ± 35	231 ± 10	433 ± 34	0.5 ± 0.1	5.1 ± 1.2	42 ± 5	23 ± 2	83.2 ± 3.9	11 ± 2	19 ± 3	22 ± 1	11 ± 1	16 ± 8	24 ± 12
	CMW_{NP}	3.5%	253 ± 13	234 ± 10	259 ± 16	0.9 ± 0.1	19.9 ± 1.1	18 ± 5	23 ± 2	69.3 ± 3.4	4 ± 1	18 ± 3	21 ± 1	11 ± 1	6 ± 6	32 ± 14
	$STMW_{NP}$	0.2%	207 ± 36	111 ± 6	141 ± 39	0.8 ± 0.3	18.4 ± 1.3	0 ± 0	12 ± 2	66.1 ± 22.1	0 ± 0	16 ± 19	26 ± 1	12 ± 1	0 ± 6	26 ± 20
Intermediate	MW	0.2%	1276 ± 354	84 ± 9	133 ± 42	0.6 ± 0.3	9.5 ± 1.6	3 ± 7	5 ± 4	72.2 ± 14.2	1 ± 2	7 ± 8	27 ± 1	12 ± 2	1 ± 35	10 ± 38
(500–1500 m)	SAMW	8.0%	719 ± 42	72 ± 6	214 ± 26	0.3 ± 0.1	23.1 ± 0.9	13 ± 3	7 ± 1	136.9 ± 57.6	5 ± 2	13 ± 3	31 ± 1	14 ± 1	6 ± 6	18 ± 13
	$AAIW_{3.1}$	4.5%	1317 ± 108	134 ± 5	499 ± 50	0.27 ± 0.04	26.8 ± 1.4	35 ± 5	9 ± 1	154.2 ± 65.1	13 ± 2	14 ± 3	27 ± 1	13 ± 1	17 ± 8	13 ± 12
	$AAIW_{5.0}$	2.9%	677 ± 36	128 ± 8	228 ± 13	0.56 ± 0.07	29.3 ± 1.4	17 ± 4	10 ± 1	102.1 ± 7.0	6 ± 2	14 ± 6	26 ± 1	12 ± 1	8 ± 9	16 ± 18
	NPIW	5.9%	671 ± 65	255 ± 6	571 ± 39	0.45 ± 0.04	22.5 ± 0.8	47 ± 5	23 ± 1	93.6 ± 4.0	12 ± 2	20 ± 3	21 ± 0	11 ± 0	20 ± 6	27 ± 12
Abyssal	CDW	27.0%	2412 ± 76	183 ± 4	821 ± 22	0.22 ± 0.01	26.7 ± 0.4	52 ± 2	12 ± 1	118.2 ± 5.5	16 ± 1	15 ± 3	25 ± 0	12 ± 0	26 ± 3	13 ± 5
(>1500 m)	$NADW_{2.0}$	12.9%	3279 ± 66	88 ± 2	467 ± 13	0.19 ± 0.01	24.7 ± 0.6	12 ± 2	6 ± 1	78.5 ± 2.6	4 ± 1	9 ± 4	25 ± 0	13 ± 0	5 ± 3	10 ± 6
	$NADW_{4.6}$	7.6%	1582 ± 99	103 ± 4	277 ± 13	0.37 ± 0.03	26.1 ± 0.9	13 ± 3	6 ± 1	89.5 ± 3.9	4 ± 1	9 ± 3	26 ± 1	12 ± 0	5 ± 5	9 ± 8
	AABW	4.4%	3780 ± 64	149 ± 6	745 ± 47	0.20 ± 0.02	28.1 ± 1.1	42 ± 5	8 ± 1	118.3 ± 5.7	14 ± 3	14 ± 19	26 ± 1	13 ± 1	25 ± 8	8 ± 12

[a]EDW: Eighteen Degrees Water, $ENACW_{12}$: Eastern North Atlantic Central Water (12°C), $ENACW_{15}$: Eastern North Atlantic Central Water (15°C), 13EqAtl: Equatorial Atlantic Central Water (13°C), $SACW_{12}$: South Atlantic Central Water (12°C), $SACW_{18}$: South Atlantic Central Water (18°C), $STMW_I$: Indian Subtropical Mode Water, ICW_{13}: Indian Central Water (13°C), $STMW_{SP}$: South Pacific Subtropical Mode Water, $SPCW_{20}$: South Pacific Central Water (20°C), 13EqPac: Equatorial Pacific Central Water (13°C), CMW_{NP}: North Pacific Central Mode Water (12°C), $STMW_{NP}$: North Pacific Subtropical Mode Water (16°C), MW: Mediterranean Water, SAMW: Sub-Antarctic Mode Water, $AAIW_{3.1}$: Antarctic Intermediate Water (3.1°C), $AAIW_{5.0}$: Antarctic Intermediate Water (5.0°C), NPIW: North Pacific Intermediate Water, $CDW_{1.6}$: Circumpolar Deep Water, $NADW_{2.0}$: North Atlantic Deep Water (2°C), $NADW_{4.6}$: North Atlantic Deep Water (4.6°C), and AABW: Antarctic Bottom Water. $\%VOL_i$ is the contribution of WT i to the total volume of water sampled during the Malaspina circumnavigation, Z_i is the archetypal depth, AOU_i is the archetypal apparent oxygen utilization, τ_i is the archetypal ideal age, OUR_i is the archetypal oxygen utilization rate, NO_{3i} is the archetypal nitrate concentration, $a_{Ch\text{-}UV}$ is the absorption coefficient of the UV chromophore at λ_{302} and $\sigma_{Ch\text{-}UV}$ of 26 nm. $a_{Ch\text{-}VIS}$ is the absorption coefficient of the VIS chromophore at λ_{415} and $\sigma_{Ch\text{-}VIS}$ of 27 nm. a_{UVi}/a_{302i} and a_{VISi}/a_{415i} are the contributions of the chromophores signal with respect to the total absorption at that specific wavelength. $Sc_{275-295}$ is the spectral slope at 275–295 nm without the UV chromophore. $Sc_{350-400}$ is the spectral slope at 350–400 nm without the VIS chromophore. A percent of increment in Sc compared to the Helms' slopes [see *Catalá et al.*, 2015]. A total of 18 water masses were identified during the Malaspina 2010 circumnavigation. Since ENACW, SACW, AAIW, and NADW are defined by two water types (WT), the total amount of water types (WT) is 22.

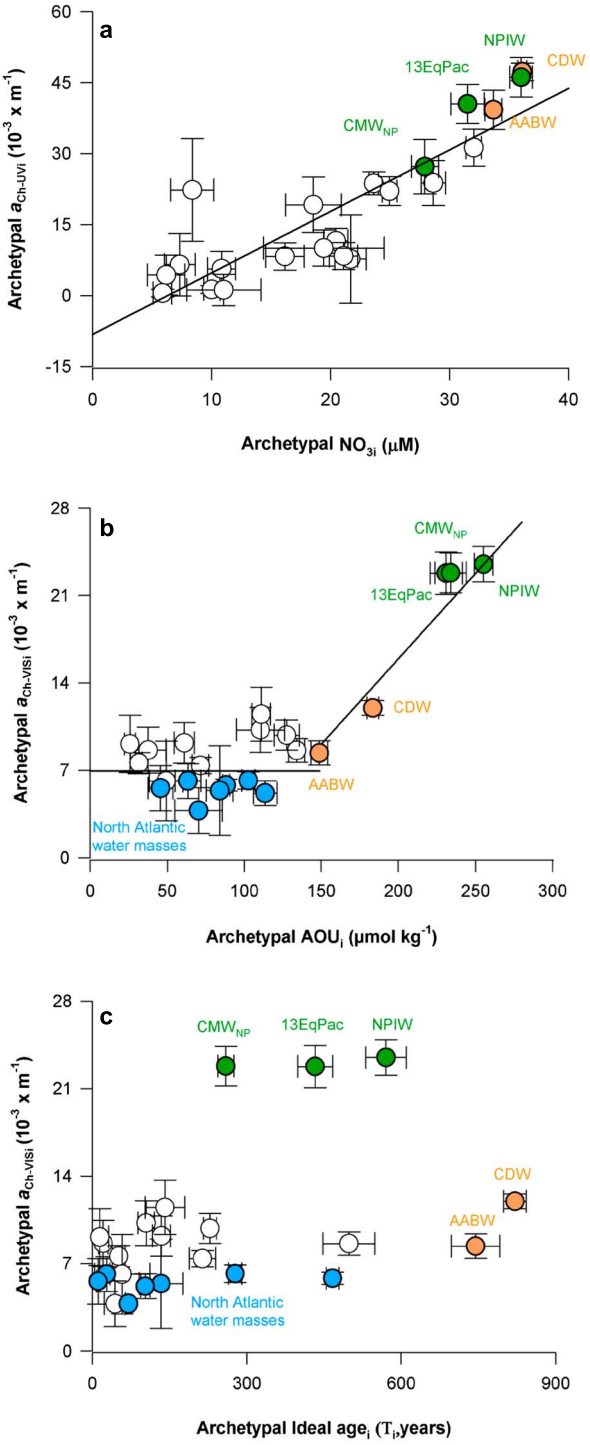

Figure 2. Relationships of the UV chromophore with nitrate and VIS chromophore with the apparent oxygen utilization and ideal age in the dark global ocean. (a) Archetypal absorption coefficient of the UV chromophore ($a_{Ch\text{-}UVi}$, $\times 10^{-3}$ m^{-1}) versus archetypal nitrate concentration (NO_{3i}, μM, black line). Archetypal absorption coefficient of the visible chromophore ($a_{Ch\text{-}VISi}$, $\times 10^{-3}$ m^{-1}) versus (b) archetypal apparent oxygen utilization (AOU_i, μmol kg^{-1}) and (c) archetypal ideal age (τ_i, years). $N = 22$. The corresponding standard deviations of the estimates are shown. Green, orange, and blue dots are water masses with distinctive characteristics (see the text for clarification).

spreads at about 1000 m in the North Atlantic. The most abundant intermediate water sampled during the circumnavigation was the Antarctic Intermediate Water (AAIW), which represented 7.4% of the total sampled volume. Finally, abyssal waters are formed at polar latitudes, either in the Northern North Atlantic or the Southern Ocean. Both intermediate and abyssal waters occupy extensive oceanic regions, being unrestricted to a determined ocean basin. The Circumpolar Deep Water (CDW) and the North Atlantic Deep Water (NADW) are the most abundant WT, representing 27% and 20% of the total sampled volume, respectively. CDW originates in the Antarctic Circumpolar Current and NADW in the Northern North Atlantic.

3.2. DOM Chromophores

A careful examination of the absorption coefficient spectra of the samples revealed a consistent and recurrent presence of two discrete absorption chromophores (Figure S1a). The first chromophore is centered at 302 nm occupying a wavelength band of 26 nm. The absorption coefficient of this UV chromophore, $a_{Ch\text{-}UV}$, ranged from 0 to 171×10^{-3} m^{-1}, with maximum values in the intermediate and abyssal waters of the Pacific Ocean (Figure 1c). The second chromophore presented a maximum absorption at 415 nm and a wavelength band of 27 nm. Maximum values of the absorption coefficient of this chromophore, $a_{Ch\text{-}VIS}$, were also found at intermediate depths of the North Pacific reaching up to 42×10^{-3} m^{-1} (Figure 1d).

3.2.1. UV Chromophore ($a_{Ch\text{-}UVi}$)

The highest $a_{Ch\text{-}UVi}$ values for the UV chromophore were $52 \pm 2 \times 10^{-3}$ m^{-1} for the CDW, $47 \pm 5 \times 10^{-3}$ m^{-1} for the North Pacific Intermediate Water (NPIW), $42 \pm 5 \times 10^{-3}$ m^{-1} for the 13EqPac, and $42 \pm 5 \times 10^{-3}$ m^{-1} for the Antarctic Bottom Water (AABW) (Table 1, orange and green dots in Figure 2a). Note that these are the less ventilated water masses sampled during the circumnavigation (as shown from their estimated ideal ages, τ) and exhibit the largest cumulative microbial respiration (as follows from their apparent oxygen utilization, AOU) (Table 1). The lowest

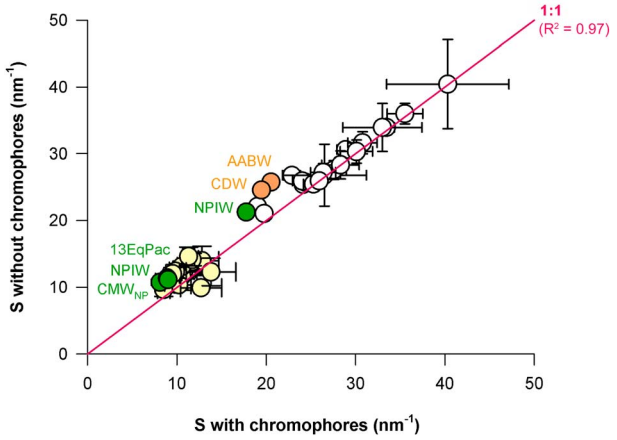

Figure 3. Comparison of the archetypal Helms' spectral slope values $S_{275-295}$ (white dots) and $S_{350-400}$ (yellow dots) with and without the UV and VIS chromophores spectra, respectively. Green and orange dots are water masses with distinctive characteristics (see the text for clarification).

values were observed in the central waters of the three ocean basins (Figure 1c). The water masses with minimum $a_{Ch\text{-}UVi}$ values were the subtropical mode waters of the Indian ($STMW_I$, $1 \pm 1 \times 10^{-3}\,m^{-1}$) and South Pacific Oceans ($STMW_{SP}$, $1 \pm 3 \times 10^{-3}\,m^{-1}$) and the Indian Central Water of 13°C (ICW_{13}, $1 \pm 1 \times 10^{-3}\,m^{-1}$), which in turn are the most ventilated water masses sampled during the circumnavigation (Table 1).

This UV chromophore is due to the absorption of nitrate in the UVB region of the spectrum [*Johnson and Coletti*, 2002]. Nitrate has two principal absorption bands, the first is an intense $\pi \rightarrow \pi^*$ band occurring in the far UV at 201 nm, while the second is a weak absorption band centered at 302 nm [*Jankowski et al.*, 1999], which coincides in position and shape with the UV chromophore (Figure S1c). In fact, addition of sodium nitrate to seawater causes an initial increase in the absorption coefficient for wavelengths <330 nm associated with the absorption properties of nitrate in the UVB region of the spectrum [*Swan et al.*, 2012]. However, an overall lack of correlation between the concentration of nitrate and the absorption coefficient of CDOM at 300 nm has been reported in the global ocean [*Nelson et al.*, 2007; *Swan et al.*, 2012]. Consistently, the relationship between the archetypal concentration of nitrate (NO_{3i}) and the archetypal absorption coefficient of CDOM at 302 nm (a_{302i}) for the water masses sampled during the circumnavigation was not significant ($R^2 = 0.12$, $p > 0.11$; data not shown). However, it is noticeable that the linear relationship of NO_{3i} with $a_{Ch\text{-}UVi}$ is highly significant ($R^2 = 0.72$, $p < 0.001$; black line in Figure 2a), indicating that the lack of correlation between NO_3 and a_{302} is simply due to the fact that humic substances are causing most of the variability of the absorption coefficient of CDOM at that specific wavelength. Furthermore, the slope of the relationship between $a_{Ch\text{-}UVi}$ and NO_{3i}, $15 \pm 2\,M^{-1}\,cm^{-1}$ is not significantly different from the molar absorption coefficient of the secondary absorption peak of nitrate in milli-Q water at 302 nm ($7\,M^{-1}\,cm^{-1}$ in the decadal scale [*Jankowski et al.*, 1999] or $16.12\,M^{-1}\,cm^{-1}$ in the Naperian scale that we use). Furthermore, the UV chromophore spectrum resembles the real nitrate spectrum (Figure S1c). This means that nitrate is the main responsible for the UV chromophore absorption.

Comparison of the Helms' $S_{275-295}$ spectral slopes of the measured spectra [see *Catalá et al.*, 2015] with those calculated by subtracting the absorption spectrum of the UV chromophore, $Sc_{275-295}$, yielded that on average, the slopes increased by 13.3 ± 6.0% when the chromophore is subtracted, reaching maximum increases of 26 ± 3% for CDW, 25 ± 8% for AABW, and 20 ± 6% for NPIW (Figure 3). This means that the microbial production of CDOM is not the only reason behind the decrease of the spectral slopes in aged ocean waters [*Helms et al.*, 2008] but the microbial production of nitrate, too. Conversely, the higher spectral slopes of the recently formed central water masses (i.e., $STMW_I$, $STMW_{SP}$, or ICW_{13}) are partly due to photodegradation of CDOM previous to water mass formation, which conducts to ammonium rather than nitrate production [*Stedmon et al.*, 2007]. Note that ammonium absorbs at much shorter wavelengths than nitrate and, therefore, do not contribute to modify the $S_{275-295}$ spectral slope.

On average, $a_{Ch\text{-}UV}$ represented 8.5 ± 1.3% of the total absorption coefficient at 302 nm, with maximum contributions of 16 ± 1% for CDW, 14 ± 3% for AABW, and 13 ± 2% for $AAIW_{3.1}$. We recommend subtracting the UV chromophore from the measured absorption spectrum in samples with $[NO_3^-]/a_{302}$ ratio > 70 μM m to consider only the effect of CDOM on the $S_{275-295}$ spectral slopes. For higher values of the ratio, the impact of NO_3^- on this slope is significant (Table 1).

Calculating the contribution of $a_{Ch\text{-}UV}$ to the total absorption at 325 nm, the standard wavelength used in biogeochemical studies in the oceans [*Nelson et al.*, 2010; *Catalá et al.*, 2015], we obtained that approximately 8.7

± 1.3% of the signal is attributable to the Ch-UV, with the maximum values around 15% in the same Antarctic abyssal and intermediate WTs as above. The subtraction of the UV chromophore from the total absorption spectra results in a decrease of 23.9% of the slope of the relationship between AOU and a_{325} obtained by *Catalá et al*. [2015]. Consideration of the second term of equation (2) into the model of the absorption coefficient spectra improves the root-mean-square error of the adjustment by 10.6 ± 1.7% on average. The improvement exceeds 15% for the water masses of the Antarctic and Pacific Oceans.

3.2.2. Visible Chromophore ($a_{\text{Ch-VIS}}$)

The visible chromophore has been previously found in subsurface waters of the eastern Atlantic Ocean, the West Pacific, and the Santa Barbara Channel [*Röttgers and Koch*, 2012] and the Arabian Sea [*Breves et al*., 2003]. It was more pronounced in and below the deep chlorophyll maximum (DCM) and extended into the oxygen minimum layer [*Röttgers and Koch*, 2012; *Breves et al*., 2003]. Here we provide further evidence of the presence of this chromophore in the dark global ocean. Maximum archetypal $a_{\text{Ch-VIS}}$ values were observed in the poorly ventilated NPIW, North Pacific Central Mode Water (CMW_{NP}), and 13EqPac, with values around $23 \pm 1 \times 10^{-3}\ \text{m}^{-1}$ (Table 1, green dots in Figures 2b and 2c). The lowest values were recorded in the central, intermediate, and abyssal waters of the North Atlantic, ranging from 5 to $9 \times 10^{-3}\ \text{m}^{-1}$ (Table 1, blue dots in Figures 2b and 2c). The scatterplot between $a_{\text{Ch-VIS}i}$ and AOU_i (Figure 2b) indicates that for $\text{AOU}_i < 150\ \mu\text{mol kg}^{-1}$, $a_{\text{Ch-VIS}i}$ remains constant at $7 \pm 1 \times 10^{-3}\ \text{m}^{-1}$, and for $\text{AOU}_i > 150\ \mu\text{mol kg}^{-1}$ a significant positive linear relationship ($R^2 = 0.95$, $p < 0.001$) was observed between $a_{\text{Ch-VIS}i}$ and AOU_i (Figure 2b). Conversely, we did not find a significant relationship between $a_{\text{Ch-VIS}i}$ and τ_i (Figure 2c), which means that aging, but not age, is the key factor controlling the accumulation of this chromophore in the dark global ocean. As AOU_i was the only explanatory variable, the water mass weighted average net production rate of $a_{\text{Ch-VIS}}$ was $3.7 \pm 0.5 \times 10^{-5}\ \text{m}^{-1}\ \text{yr}^{-1}$ and was obtained as

$$\text{NP}a_{\text{Ch-VIS}} = \sum_i \frac{\text{VOL}_i}{100} \cdot \left(\frac{\partial a_{\text{VIS}i}}{\partial \text{AOU}_i}\right) \cdot \left(\frac{\partial \text{AOU}_i}{\partial \tau_i}\right) = \sum_i \frac{\text{VOL}_i}{100} \cdot \left(\frac{\partial a_{\text{VIS}i}}{\partial \text{AOU}_i}\right) \cdot \text{OUR}_i \quad (3)$$

Dividing this number by the average absorption coefficient of $a_{\text{Ch-VIS}}$ ($10.9 \pm 0.9 \times 10^{-3}\ \text{m}^{-1}$), we obtained a turnover time of 292 ± 61 years for this chromophore, which is significantly shorter ($p < 0.05$) than the turnover time of the total humic fraction of CDOM, 634 ± 120 years, as calculated from the absorption coefficient at 325 nm (a_{325}) [*Catalá et al*., 2015].

The respiratory enzyme cytochrome c oxidase (CcO) has been suggested as a plausible source for the absorption of the visible chromophore [*Röttgers and Koch*, 2012]. This enzyme presents an absorption maxima around 410 to 415 nm (Figure S1c) and is one of the most important components of cellular respiration, which reduces molecular oxygen to water coupled to the pumping of protons across the mitochondrial or bacterial membrane [*Yoshikawa et al*., 2011]. CcO presents a Soret band ($\pi \rightarrow \pi^*$ transition located mainly on porphyrin) centered at 410 nm (decadic molar absorption coefficient of $106 \cdot 10^3\ M^{-1}\ \text{cm}^{-1}$) in the oxidized protein and at 415 nm in the reduced form. Furthermore, it presents a Q band centered at 530 nm (decadic molar absorption coefficient of $11.2\ 10^3\ M^{-1}\ \text{cm}^{-1}$) in the oxidized form and at 520 and 550 nm in the reduced form [*Moore and Pettigrew*, 1990]. The relationship of the molar absorption coefficient of CcO with the $a_{\text{Ch-VIS}}$ allows estimating an apparent CcO concentration range between 0.2 and 1 n*M* (Figure S1c). These concentrations were obtained by dividing $a_{\text{Ch-VIS}}$ by the Naperian molar absorption coefficient of CcO (i.e., $244\ 10^3\ M^{-1}\ \text{cm}^{-1}$ for the oxidized form of CcO).

Previous studies demonstrated absorption at 415 nm by biodetritus [*Kishino et al*., 1985; *Bricaud and Stramski*, 1990] and by heterotrophs such as bacteria, ciliates, and flagellates [*Morel and Ahn*, 1990; *Stramski and Kiefer*, 1998]. Hence, it is probable that a noteworthy source of this chromophore originates from the particulate fraction, from either bacteria or detrital particles sinking down from the euphotic zone [*Röttgers and Koch*, 2012]. Likewise, the stable $a_{\text{Ch-VIS}i}$ values around $7 \pm 1 \times 10^{-3}\ \text{m}^{-1}$ for water masses with $\text{AOU}_i < 150\ \mu\text{mol kg}^{-1}$ may be CcO remnants produced by phytoplankton during respiration and accumulated in the surface layer due to their slow degradation rates until water mass formation during winter mixing.

Comparing the measured Helms' $S_{350-400}$ and S_R spectral slopes [see *Catalá et al*., 2015] with those calculated by subtracting the $a_{\text{Ch-VIS}}$ chromophore spectra, we obtained that the slopes increased by 14.8 ± 10.6% when the chromophore is subtracted, reaching maximum increases of 32 ± 14% for CMW_{NP}, 27 ± 12% for NPIW and 24 ± 12% for 13 EqPac (Figure 3). On average, the $a_{\text{Ch-VIS}}$ represented 13.6 ± 4.1% of the total absorption

coefficient at 415 nm, with maximum contributions of 20 ± 3% for NPIW, 19 ± 3% for 13EqPac, and 18 ± 3% for CMW_{NP}. Consideration of the second term of equation (2) into the model of the absorption coefficient spectra improves the root-mean-square error of the adjustment by 12.7 ± 1.7% on average. The improvement exceeds 30% for the NIPW, 13EqPac, and CMW_{NP}. The effect of both UV and visible chromophores on general slopes of wide range, such as the slope at 250–500 nm—$S_{250-500}$—is negligible (Table S1).

4. Conclusions

In this work, we have developed a MATLAB toolbox to deconvolve the signal attributed to the UV and VIS chromophores from the exponential decay curve characteristic of humic substances, estimated the contribution of the $a_{Ch\text{-}UV}$ and $a_{Ch\text{-}VIS}$ to the total absorption signal, and compared the effect of the two identified chromophores on the Helms' spectral slopes of the measured spectra. Likewise, the recent method proposed by *Massicotte and Markager* [2016] allows obtaining robust estimates of spectral slopes that are independent of the spectral range used, which facilitates the comparison among studies. Here we propose nitrate as a certain generator of the UV chromophore. Its impact on the slope $S_{275-295}$ and on the absorption coefficients at 302 nm and 325 nm was more pronounced for the Antarctic abyssal and intermediate WTs. We assigned the visible chromophore to CcO, which is considered a residue released after cell ruptures. The fact that only aging contributed to explain the global distribution of $a_{Ch\text{-}VIS}$ reflects that this chromophore is more dependent on the cumulative respiration than on the time that the water mass has not been in contact with the atmosphere. Its impact on the slope $S_{350-400}$ and on the absorption coefficient at 415 nm was more substantial in the poorly ventilated central and intermediate waters of the North Pacific Ocean. Regarding the contribution of nitrate to the absorption spectrum of seawater, we propose the removal of the spectrum of nitrate from the total spectrum of seawater either by subtracting the measured molar absorption spectrum of nitrate multiplied by the nitrate concentration of the samples or by using the statistical approach proposed in this work. To only consider the chromophoric fraction of DOM, the absorption spectra of nitrate should be subtracted in samples with a $[NO_3^-]$:a_{302} ratio $> 70\ \mu M$ m.

Acknowledgments

We thank C.M. Duarte for the coordination of the Malaspina expedition; the chief scientists of the seven legs, the staff of the Marine Technology Unit (CSIC-UTM), and the Captain and crew of R/V *Hespérides* for their outright support during the circumnavigation. Also, we thank the Physics block for collecting, calibrating, and processing the CTD data; Dolors Blasco for facilitating the nitrate data; Antonio Fuentes-Lema, Eva Ortega-Retuerta, Celia Marrasé, Mar Nieto-Cid, Cristina Romera-Castillo, and Francesca Iuculano for their contribution to sampling collection and measurements; Bieito Fernandez-Castro for MATLAB support, and Eulogio Corral Arredondo for the "Chromophores Toolbox" Web page design. We also acknowledge the valuable comments and criticisms of two anonymous reviewers. This study was financed by the Malaspina 2010 circumnavigation expedition (grant CSD2008-00077). The data used are listed in Table 1, and the "Chromophores Toolbox" to estimate the UV and Visible chromophores is available at the Web page "http://ecologia.ugr.es/pages/herramientas/toolbox-matlab?lang=en".

References

Álvarez-Salgado, X. A., M. Nieto-Cid, M. Álvarez, F. F. Pérez, P. Morin, and H. Mercier (2013), New insights on the mineralization of dissolved organic matter in central, intermediate, and deep water masses of the northeast North Atlantic, *Limnol. Oceanogr.*, *58*, 681–696.

Benner, R., and G. J. Herndl (2011), Bacterially derived dissolved organic matter in the microbial carbon pump, in *Microbial Carbon Pump in the Ocean*, edited by N. Jiao, F. Azam, and S. Sanders, pp. 46–48, Science/AAAS, Washington, D. C.

Benson, B. B., and s (1984), The concentration and isotopic fractionation of oxygen dissolved in freshwater and seawater in equilibrium with the atmosphere, *Limnol. Oceanogr.*, *29*, 620–632.

Breves, W., R. Heuermann, and R. Reuter (2003), Enhanced red fluorescence emission in the oxygen minimum zone of the Arabian Sea, *Ocean. Dyn.*, *53*, 86–97, doi:10.1007/s10236-003-0026-y.

Bricaud, A., and D. Stramski (1990), Spectral absorption coefficients of living phytoplankton and nonalgal biogenous matter: A comparison between the Peru upwelling area and the Sargasso Sea, *Limnol. Oceanogr.*, *35*, 562–582.

Bricaud, A., A. Morel, and L. Prieur (1981), Absorption by dissolved organic matter of the sea (yellow substance) in the UV and visible domains, *Limnol. Oceanogr.*, *26*, 43–53.

Catalá, T. S., et al. (2015), Water mass age and aging driving chromophoric dissolved organic matter in the dark global ocean, *Global Biogeochem. Cycles*, *29*, 917–934, doi:10.1002/2014GB005048.

Grasshoff, K., K. Kremling, and M. Ehrhardt (1999), *Methods of Seawater Analysis*, Wiley-VCH.

Green, S. A., and N. V. Blough (1994), Optical absorption and fluorescence properties of chromophoric dissolved organic matter in natural waters, *Limnol. Oceanogr.*, *39*, 1903–1916.

Hansell, D. A., and C. A. Carlson (2013), Localized refractory dissolved organic carbon sinks in the deep ocean, *Global Biogeochem. Cycles*, *27*, 705–710, doi:10.1002/gbc.20067.

Helms, J. R., A. Stubbins, J. D. Ritchie, E. C. Minor, D. J. Kieber, and K. Mopper (2008), Absorption spectral slopes and slope ratios as indicators of molecular weight, source, and photobleaching of chromophoric dissolved organic matter, *Limnol. Oceanogr.*, *53*, 955–969.

Jankowski, J. J., D. J. Kieber, and K. Mopper (1999), Nitrate and nitrite ultraviolet actinometers, *Photochem. Photobiol.*, *70*(3), 319–328.

Jenkins, W. J. (1982), Oxygen utilization rates in the North Atlantic subtropical gyre and primary production in oligotrophic systems, *Nature*, *300*, 246–249.

Jiao, N., et al. (2010), Microbial production of recalcitrant dissolved organic matter: Long-term carbon storage in the global ocean, *Nat. Rev. Microbiol.*, *8*, 593–599.

Johnson, K. S., and L. J. Coletti (2002), In situ ultraviolet spectrophotometry for high resolution and long-term monitoring of nitrate, bromide and bisulfide in the ocean, *Deep Sea Res., Part I*, *49*, 1291–1305.

Khatiwala, S., F. Primeau, and T. Hall (2009), Reconstruction of the history of anthropogenic CO_2 concentrations in the ocean, *Nature*, *462*, 346–349.

Khatiwala, S., F. Primeau, and M. Holzer (2012), Ventilation of the deep ocean constrained with tracer observations and implications for radiocarbon estimates of ideal mean age, *Earth Planet. Sci. Lett.*, *325–326*, 116–125.

Kishino, M., M. Takahashi, N. Okami, and S. Ichimura (1985), Estimation of the spectral absorption coefficients of phytoplankton in the sea, *Bull. Mar. Sci.*, *37*, 634–642.

Lechtenfeld, O. J., N. Hertkorn, Y. Shen, M. Witt, and R. Benner (2015), Marine sequestration of carbon in bacterial metabolites, *Nat. Commun.*, *6*, 6711, doi:10.1038/ncomms7711.

Massicotte, P., and S. Markager (2016), Using a Gaussian decomposition approach to model absorption spectra of chromophoric dissolved organic matter, *Mar. Chem.*, *180*, 24–32.

Moore, G. R., and G. W. Pettigrew (1990), *Cytochromes C, Evolutionary, Structural and Physicochemical Aspect*, pp. 1–478, Academic Press, London.

Morel, A., and Y.-H. Ahn (1990), Optical efficiency factors of free-living marine bacteria: Influence of bacterioplankton upon the optical properties and particulate organic carbon in oceanic waters, *J. Mar. Res.*, *48*, 145–175.

Nelson, N. B., D. A. Siegel, and A. F. Michaels (1998), Seasonal dynamics of colored dissolved material in the Sargasso Sea, *Deep Sea Res., Part I*, *45*, 931–957.

Nelson, N. B., D. A. Siegel, C. A. Carlson, C. M. Swan, W. M. Smethie Jr., and S. Khatiwala (2007), Hydrography of chromophoric dissolved organic matter in the North Atlantic, *Deep Sea Res., Part I*, *54*, 710–731.

Nelson, N. B., D. A. Siegel, C. A. Carlson, and C. M. Swan (2010), Tracing global biogeochemical cycles and meridional overturning circulation using chromophoric dissolved organic matter, *Geophys. Res. Lett.*, *37*, L03610, doi:10.1029/2009GL042325.

Ogawa, H., Y. Amagai, I. Koike, K. Kaiser, and R. Benner (2001), Production of refractory dissolved organic matter by bacteria, *Science*, *292*, 917–920.

Röttgers, R., and B. P. Koch (2012), Spectroscopic detection of a ubiquitous dissolved pigment degradation product in subsurface waters of the global ocean, *Biogeosciences*, *9*, 2585–2596.

Schlitzer, R. (2016), Ocean Data View. [Available at http://odv.awi.de.]

Stedmon, C. A., and N. B. Nelson (2015), The optical properties of DOM in the ocean, in *Biogeochemistry of Marine Dissolved Organic Matter*, 2nd ed., edited by D. A. Hansell and C. A. Carlson, pp. 481–508, Academic Press, Boston.

Stedmon, C. A., S. Markager, L. Tranvik, L. Kronberg, T. Slätis, and W. Martinsen (2007), Photochemical production of ammonium and transformation of dissolved organic matter in the Baltic Sea, *Mar. Chem.*, *104*, 227–240.

Stramski, D., and D. A. Kiefer (1998), Can heterotrophic bacteria be important to marine light absorption?, *J. Plankton Res.*, *20*, 1489–1500.

Swan, C. M., N. B. Nelson, D. A. Siegel, and T. S. Kostadinov (2012), The effect of surface irradiance on the absorption spectrum of chromophoric dissolved organic matter in the global ocean, *Deep Sea Res., Part I*, *63*, 52–64.

Twardowski, M. S., E. Boss, J. M. Sullivan, and P. L. Donaghay (2004), Modeling the spectral shape of absorbing chromophoric dissolved organic matter, *Mar. Chem.*, *89*, 69–88.

Yoshikawa, S., K. Muramoto, and K. Shinzawa-Itoh (2011), Proton-pumping mechanism of cytochrome c oxidase, *Annu. Rev. Biophys.*, *40*, 205–223.